Inferring responses to climate dynamics from historical demography in neotropical forest lizards

Ivan Prates[a,b,1], Alexander T. Xue[a,b], Jason L. Brown[a,c], Diego F. Alvarado-Serrano[a,d], Miguel T. Rodrigues[e], Michael J. Hickerson[a,b,f], and Ana C. Carnaval[a,b]

[a]Department of Biology, City College of New York, New York, NY 10031; [b]Department of Biology, Graduate Center, City University of New York, New York, NY 10016; [c]Cooperative Wildlife Research Laboratory, Department of Zoology, Southern Illinois University, Carbondale, IL 62901; [d]Department of Ecology and Evolutionary Biology, University of Michigan, Ann Arbor, MI 48109; [e]Departamento de Zoologia, Instituto de Biociências, Universidade de São Paulo, São Paulo, SP 05508-090, Brazil; and [f]Division of Invertebrate Zoology, American Museum of Natural History, New York, NY 10024

We apply a comparative framework to test for concerted demographic changes in response to climate shifts in the neotropical lowland forests, learning from the past to inform projections of the future. Using reduced genomic (SNP) data from three lizard species codistributed in Amazonia and the Atlantic Forest (*Anolis punctatus*, *Anolis ortonii*, and *Polychrus marmoratus*), we first reconstruct former population history and test for assemblage-level responses to cycles of moisture transport recently implicated in changes of forest distribution during the Late Quaternary. We find support for population shifts within the time frame of inferred precipitation fluctuations (the last 250,000 y) but detect idiosyncratic responses across species and uniformity of within-species responses across forest regions. These results are incongruent with expectations of concerted population expansion in response to increased rainfall and fail to detect out-of-phase demographic syndromes (expansions vs. contractions) across forest regions. Using reduced genomic data to infer species-specific demographical parameters, we then model the plausible spatial distribution of genetic diversity in the Atlantic Forest into future climates (2080) under a medium carbon emission trajectory. The models forecast very distinct trajectories for the lizard species, reflecting unique estimated population densities and dispersal abilities. Ecological and demographic constraints seemingly lead to distinct and asynchronous responses to climatic regimes in the tropics, even among similarly distributed taxa. Incorporating such constraints is key to improve modeling of the distribution of biodiversity in the past and future.

phylogeography | population genomics | Amazon Forest | Atlantic Forest | climate change

Nearly three decades have passed since Avise (1, 2) first inspired tropical biologists to study community-level responses to regional changes through the lens of population genetics. However, despite the high species richness, endemism, and genetic structure observed in tropical regions (3), comparative phylogeographic approaches are relatively unexplored in the tropics. To date, most available phylogeographic comparisons report spatial patterns of organelle DNA variation, primarily mitochondrial, across a handful of tropical taxa (4–10). Although addressing different regions and organisms, these studies have centered on two major topics: the role of climatic discontinuities (4, 10) or rivers (5, 9) as barriers to dispersal and the influence of glacial–interglacial temperature oscillations on species ranges, a topic originally explored in studies of northern hemisphere taxa (11) but widely embraced by tropical phylogeographers worldwide (6–8). This first generation of comparative studies indicated pervasive geographic structure of mitochondrial lineages (7–9) and either congruent spatial patterns of genetic diversity across species of broadly similar ecologies (4, 7) or differences in ways largely expected, given their life history traits (6, 12). However, as tropical phylogeographers began to sample loci (13–15) and taxa (8, 10, 16) more widely, reports of asynchronous lineage diversification and distinct demographic syndromes among codistributed taxa (such as population expansions and contractions) became commonplace.

If idiosyncratic responses to common landscape changes characterize ecological communities in the tropics (17, 18) and beyond (19, 20), their incorporation in phylogeographic methods can significantly improve our understanding of the impacts of former environmental shifts on regional species pools. Methods that build upon coalescent theory to account for historical heterogeneity across taxa under a single statistical framework (21, 22) provide increased power to test concerted demographic responses at the level of ecological assemblages. These highly flexible approaches have profited from novel bench and analytical methods that build on genomic or reduced genome data, resulting in improved estimates of demographic parameters and histories (23–25). Although still rare, studies that combine coalescent-based demographic simulations and broader genomic sampling across taxa are unquestionably deepening our understanding of how tropical diversity came to be distributed (17).

Improved knowledge of species responses to climate and landscape shifts will also strengthen forecasts of community responses to future global changes. Going beyond predictions of geographic ranges under future climates (26, 27), molecular data can guide the parameterization of plausible species-specific models of the distribution of genetic diversity, and hence evolutionary potential, under predicted scenarios of global change (28). This as yet underexplored application of comparative phylogeography is especially promising and timely given today's threats to tropical ecosystems (3).

Using reduced genome data of codistributed neotropical forest taxa, we apply a comparative phylogeographic framework to address two major goals. First, we ask whether present-day patterns of genomic diversity reflect congruent, multitaxa responses to historical environmental shifts documented within and across rainforest systems (29). Then, using the distribution of suitable habitats and the molecular data to gain insight about species-specific demographic parameters (dispersal rates and population

---

densities over time), we develop plausible models of the spatial distribution of genetic diversity under future climates. To do so, we analyze SNP data from *Anolis punctatus* and *Anolis ortonii* (Dactyloidae) and from *Polychrus marmoratus* (Polychrotidae). These codistributed arboreal lizard species occur in both Amazonia and the coastal Atlantic Forest of South America but are absent from the intervening open and drier scrublands and savannahs of the Caatinga and Cerrado domains.

Instead of examining the effects of temperature fluctuations associated with glacial–interglacial cycles commonly addressed by phylogeographic studies, we focus our historical study on the influence of a recently hypothesized spatial dynamics of moisture transport in tropical South America over the last 250,000 y (29). Paleoecological studies indicate that precipitation patterns have been the major constraining element of tropical rainforest distribution during the Quaternary (30). Through a compilation of proxy data based largely on geochemical analyses of cave deposits, it has been proposed that levels of precipitation in the eastern portion of Amazonia dynamically matched those in the northern portion of the Atlantic Forest, whereas precipitation patterns in western Amazonia have been linked to those in the southern Atlantic Forest (29). These two macroclimatic systems presumably have been acting as a dipole, with multiple cycles of inversion of precipitation regimes between regions that followed the precession component of Earth's orbital cycles. For instance, although decreased rainfall has been inferred to impact eastern Amazonia and the northern Atlantic Forest ~20,000 ya, an opposite pattern (increased precipitation) is recorded for western Amazonia and the southern Atlantic Forest at that time (29). The possibility that environmental drivers other than glacial–interglacial temperature oscillations have impacted tropical biotas worldwide has important implications for phylogeographic investigations, suggesting that at least some regions in the tropics are subjected to processes fundamentally different from those in the better-known temperate regions. We ask whether this proposed out-of-phase precipitation dynamics led to contrasting phylogeographic patterns between rainforest regions, testing recently proposed hypotheses about linked biological responses to synchronous but contrasting climatic regimes in South American forests.

Our approach tests for temporal congruence of demographic trends, using coalescent simulations in combination with approximate Bayesian computation (ABC) to test for synchronous shifts in population sizes (22). We examine the timing and magnitude of population changes in different forest regions occupied by a single species as well as codistributed species within the same region. Given the geographic distribution of the three target lizard species, which are largely absent from the southern Atlantic Forest (*A. punctatus* and *P. marmoratus* occupy a limited extent of the southern Atlantic Forest in the states of Rio de Janeiro and São Paulo), we focus on concerted demographical shifts between western Amazonia, eastern Amazonia, and the northern Atlantic Forest.

Further exploring the molecular data and their potential contribution to conservation, we then expand on a recently proposed framework (28) to model the plausible distribution of genomic diversity of the two focal *Anolis* species under future climates. To illustrate this approach, we use a 2080 climate model based on the Representative Concentration Pathway (RCP) 6.0 emission scenario, which has been used extensively to represent a medium carbon emission trajectory (31) and results in midrange estimates of average global changes (32). For this analysis, we infer species-specific demographic parameters from a combination of species distribution models, forward-in-time demographic simulations, and backward-in-time coalescent simulations that are compared with the empirical SNP data. To avoid potential modeling limitations imposed by Amazonia's sparsely distributed weather stations (33), we restrict our forecasts to the highly endangered Atlantic Forest hotspot (7).

Results and Discussion

The spatial distribution of phylogenetic structure within all three species supports a scenario of colonization of the Atlantic Forest from the Amazonian domain (Fig. 1 and Datasets S1–S3). This pattern is consistent with the hypothesis that former increase in precipitation promoted rainforest expansion and facilitated biotic exchange between Amazonia and the Atlantic Forest during the Quaternary (29). It also agrees with patterns of phylogeographic structure reported for other vertebrate taxa (34–36). In all species, we found that samples from the Atlantic Forest are monophyletic and are nested among Amazonian lineages, and more closely related to lizards from eastern than from western Amazonia (although the relationship is weakly supported for *A. ortonii* and *P. marmoratus*; Fig. 1). Nonetheless, spatial patterns of population genetic structure, inferred by a clustering algorithm (37), differ across taxa (Fig. 1): *P. marmoratus* is recovered as largely panmictic, *A. ortonii* is composed of two genetic clusters (Atlantic Forest and Amazonia), and three clusters are recognized within *A. punctatus* (western Amazonia near the Brazil–Peru border, Southwestern and Central Amazonia, and eastern Amazonia plus the Atlantic Forest).

Species Show Different Historical Demographic Syndromes. Demographic analyses across spatial groups within each species recover signals of population size shifts in western Amazonia, eastern Amazonia, and the northern Atlantic Forest. However, the demographic scenarios that best fit the genomic data, as well as the estimated time of demographic change, differed across species. These observations are in disagreement with the expectations of biological responses to out-of-phase climate dynamics as described above (29). In the case of *A. punctatus*, the best-fit demographic syndrome (38) infers a scenario of population expansion [posterior probability (PP) ≥0.98] in each of the three regions, with an ~8- to 17-fold expansion dating to ~62 kya in western Amazonia [95% credibility interval (CI) = 15–124 kya; see Dataset S4 for posterior estimates of all model parameters; posterior estimates of all model parameters had well-defined peak-shaped distributions; see plots in Fig. S1–S4], to ~120 kya in eastern Amazonia (CI = 34–207 kya), and to ~60 kya in northern Atlantic Forest (CI = 14–118 kya). The analyses of *A. ortonii* support an ~10- to 12-fold population contraction in all three regions (PP ≥0.88) dating to ~240 kya in western Amazonia (CI = 12–907 kya), to ~204 kya in eastern Amazonia (CI = 9–863 kya), and to ~81 kya in northern Atlantic Forest (CI = 10–300 kya). A scenario of an ~14-fold population contraction at ~72 kya (CI = 11–256 kya) was supported for *P. marmoratus* in the Atlantic Forest (PP = 1.0), the only region with sufficient sampling of SNPs per individual to enable historical demographic inference in this species.

Shifts in Population Size Are Asynchronous. Extending beyond region-specific inferences of population size change within each species, we applied hierarchical demographic models to combine data across regions and species and test for assemblage-wide synchrony in population shifts. To implement this multiregion, multitaxon framework, we used the aggregate site frequency spectrum (aSFS) to summarize patterns of genetic variation across groups and coupled it with coalescent simulations and a hierarchical approximate Bayesian computation (hABC) approach that allows species-specific parameters to vary independently (22). In an analysis that combined data from both *A. punctatus* and *A. ortonii* in all regions (western Amazonia, eastern Amazonia, and northern Atlantic Forest), we recovered a signal of largely asynchronous demographic change [dispersal index, the variance/mean of the time of population size change (DI) = 76,549; proportion of groups in a synchronous pulse (ζ) = 0.50; Dataset S5 and Fig. S5]. A joint analysis restricted to the northern Atlantic Forest, where sufficient sampling of SNPs per individual is also available for *P. marmoratus*, supports a scenario of partially synchronous population size changes
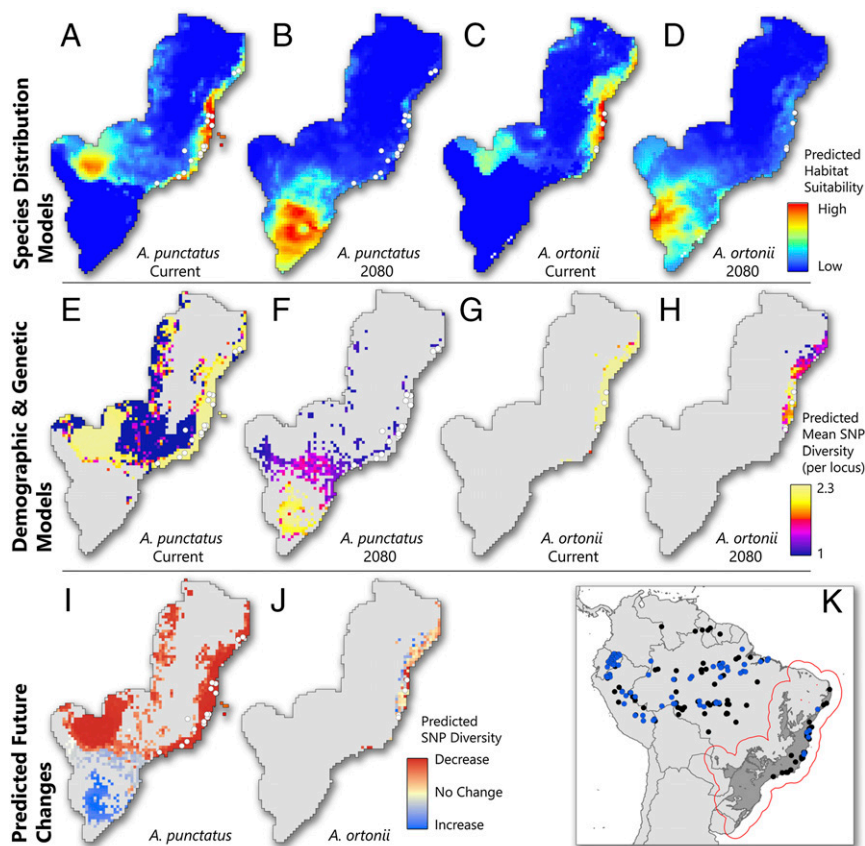
Fig. 1. Phylogenetic relationships between sampled individuals. Relationships for *A. punctatus* (*A* and *D*), *A. ortonii* (*B* and *E*), and *P. marmoratus* (*C* and *F*) were inferred through SVD quartets (42) based on unlinked SNP data. Asterisks denote bootstrap support >0.70. Bars to the right of trees represent population genetic structure, inferred through sNMF (37). Western Amazonian samples are indicated in blue, eastern Amazonian samples in orange, and Atlantic Forest samples in pink. In the case of western Amazonian *A. punctatus*, two distinct genetic populations (light and dark blue) were inferred with sNMF. Given the availability of samples, and to avoid combining different genetic populations in a single spatial group, we did not include the western Amazonia samples indicated by dark blue in our demographic analyses.

across the three lizard taxa (DI = 17,361; ζ = 0.67). These asynchronous or partially synchronous responses across species are consistent with the results of multiregion analyses conducted within each taxon separately. In a multiregion analysis restricted to *A. ortonii*, the data are consistent with a pattern of partially synchronous contractions, suggesting that two of the three regions responded in synchrony (DI = 41,314; ζ = 0.67). In *A. punctatus*, however, we detected a strong signal of synchronous population size shifts across all geographic regions, with coexpansion happening at ~119 kya [DI = 0.0; ζ = 1.0].

Although the population-level analyses largely support the occurrence of population changes within the time frame of documented atmospheric moisture shifts over the past 250 ky (29), the contrasting syndromes among species (e.g., expansions in *A. punctatus* vs. contractions in *A. ortonii* and *P. marmoratus*) and the uniformity of demographic responses across forest regions and within species (in *A. punctatus* and *A. ortonii*) are inconsistent with the hypothesis that these lizards similarly tracked out-of-synchrony contractions and expansions of South America's lowland forests (29). The general similarity of within-species population responses may indicate that demographic patterns are largely determined more by species-specific biological attributes than by spatial patterns of environmental variation across time. Future analyses of biological responses to the recently proposed South American macroclimatic zones (29) will benefit from a more extensive spatial sampling, particularly in under-explored regions such as the extreme west of Amazonia and the Andean foothills, and also will profit from the inclusion of additional species.

Genetic Diversity Under Future Climates. The distinct responses to environmental shifts observed across these broadly codistributed taxa, as shown by the historical analyses, are also prevalent in predictions of the distribution of genetic diversity under future climates. Although forecast models predict severe loss of genetic diversity for both *A. punctatus* and *A. ortonii* by 2080, the projected spatial distribution of genetic diversity in these two species is markedly distinct (Fig. 2 *I* and *J*). To develop models of the plausible future spatial distribution of allelic diversity, we adapted a recently proposed framework (28) that takes into account not only the distribution of suitable habitats under future climates but also species-specific ecological and demographic constraints inferred from molecular data. This framework first uses carefully parameterized species distribution models (SDMs) to approximate the spatial distribution of suitable habitats and landscape permeability to dispersal. Then empirical genetic (here reduced genomic) data are used to approximate the maximum density of individuals and the dispersal rates across the landscape (28).

Projection of present-day SDMs (Fig. 2 *A* and *C*) onto 2080 climate predicts a dramatic decrease of suitable habitat along the current range of both species (Fig. 2 *B* and *D*), including areas where present-day levels of genetic (SNP) diversity are high (Fig. 2 *E* and *G*). On the other hand, the SDM projections into the future predict high suitability in presently cold areas of southern Brazil, where both species currently are absent. Despite such similar predicted habitat suitability, models of the plausible distribution of genetic diversity of the two species by 2080 differ dramatically (Fig. 2 *F* and *H*). For *A. punctatus*, genetic diversity is predicted to decline strongly across the northern Atlantic Forest but to increase in the south

Fig. 2. Predicted habitat suitability and genetic changes resulting from future climate change. (*A–D*) Species distribution models for the present time and 2080 for *A. punctatus* (*A* and *B*, respectively) and for *A. ortonii* (*C* and *D*, respectively). (*E–H*) Results from demographic and genetic modeling for the present time and 2080 for *A. punctatus* (*E* and *F*, respectively) and *A. ortonii* (*G* and *H*, respectively). (*I* and *J*) Projected plausible changes in genetic diversity by 2080 for *A. punctatus* (*I*) and *A. ortonii* (*J*). White dots in maps indicate the localities with empirical genetic data that were used for ABC parameter estimation. (*K*) Overview of demographic modeling extent (area enclosed by red line), SDM modeling extent along with vetted localities (blue, *A. punctatus*; black, *A. ortonii*), and historic distribution of the Atlantic Forest (depicted in dark gray).

(Fig. 2*F*). *A. ortonii* is expected to maintain some genetic diversity in the northern Atlantic Forest but is not expected to colonize the potentially new suitable habitats arising in the south (Fig. 2*H*).

Although models of species distribution under future climates have been widely used to guide conservation (26, 27), these results suggest that relevant insight can be gained by incorporating genomic data in predictive studies. A naive interpretation of the SDMs of the two *Anolis* could flag southern Brazil as highly suitable for both species by 2080 (Fig. 2 *B* and *D*), potentially preventing future loss of genetic diversity. However our spatial demographic models indicate that these regions may in fact hold genetic diversity for *A. punctatus* (Fig. 2*F*) but not for *A. ortonii* (Fig. 2*H*). Such different predictions result from contrasting population densities and capacities for dispersal: When tied to the spatial data, SNP variation in *A. punctatus* indicated that, on average, 9.97% of each grid cell's occupants may emigrate at every generation, compared with 1.23% for *A. ortonii*. Our estimates of maximum carrying capacities further suggest that *A. punctatus* can attain much higher densities of individuals than *A. ortonii* (5,563 vs. 1,181 individuals per 30 km^2; for all parameters, PP = 1) (Fig. S6 and Table S1). These results correlate well with differences in body size and perceived abundances in the field: *A. punctatus* is much larger and also is observed much more frequently than *A. ortonii* in most of the areas we sampled. Importantly, these differences are consistent with the notion that dissimilar ecological and demographic constraints lead to distinct species responses to shared environmental change and are relevant for understanding

demographic trends (28), even in species that occupy broadly similar climatic niches. Although challenging, the incorporation of species-specific ecological traits appears central to models of community responses to ongoing global change, both in the past and in the future.

Concluding Remarks

Through a comparative analysis of widely ranged and codistributed neotropical forest lizards, we find concordant spatial patterns of phylogeographic structure across taxa, an observation consistent with previous mitochondrial DNA-based studies throughout the tropics (4, 7). Similar to the relatively few studies targeting multiple loci and tropical taxa (13–15), we nonetheless find that the demographic processes underscoring those patterns vary across species. This view is supported by tests of synchronous population size shifts that allow for species-specific parameters as well as by plausible models of the distribution of genetic diversity under future carbon emissions. Taxa associated with broadly similar climatic conditions exhibit contrasting responses to common environmental changes, a scenario also supported by simulation-based macroecological studies (20).

By combining genomic data with knowledge of the distribution of past, present, and future climates, we learn that species responses to environmental shifts are likely mediated, at least in part, by taxon-specific features that can be approximated through demographic simulations and molecular inference. The use of biological data to document or refine our understanding of the

geological and climatic history of the Earth (39)—topics so fundamental to the description of the evolution of tropical biodiversity—will benefit from the incorporation of ecological differences among species. As we embark on a new genomic era, comparative phylogeography brings novel insights and exciting advances that bridge ecology and evolution and strengthens their links with the environmental sciences and conservation.

Materials and Methods

Sequencing Protocols and Phylogenetic Analyses. We generated SNPs from 43 *A. punctatus* and 23 *A. ortonii* (Dactyloidae) and from 11 *P. marmoratus* (Polychrotidae) individuals (Dataset S6). For phylogenetic inference, we included one individual of *Anolis dissimilis, Anolis fuscoauratus, Anolis phyllorhinus, Anolis tandai, Anolis trachyderma, Anolis transversalis,* and *Polychrus liogaster* as outgroups. Genomic DNA was extracted from liver or tail fragments preserved in 100% ethanol through high-salt extraction and RNase treatment. Extractions were verified on agarose gels to ensure that the DNA was not degraded. DNA concentration was measured in a Qubit 2 fluorometer (Invitrogen) to ensure a final concentration of 30–100 ng DNA/μL in a total volume of 30 μL [in Tris EDTA buffer (Thermo Fisher Scientific, Waltham)].

We generated a restriction site-associated DNA library through genotype-by-sequencing (40) at the Institute of Biotechnology at Cornell University. Genomic DNA was first reduced to a representation library using the EcoT22I restriction enzyme. Resulting fragments were tagged with individual barcodes, PCR-amplified, multiplexed, and sequenced in an Illumina HiSeq platform (38). The number of total single-end reads per individual ranged from ~300,000 to 6.3 million. We used a Pyrad 3.0.6 pipeline (41) to demultiplex and assign reads to individuals based on sequence barcodes, to perform de novo read assembly (clustering similarity threshold >0.9), to align reads into loci, and to identify SNPs and genotypes. We enforced a minimum Phred quality score (33) and minimum sequence coverage (10×) to filter out poor-quality reads and reduce base-calling error. To reduce potential paralogs, we enforced a maximum number of heterozygous individuals per DNA site ($n = 5$). Final locus length ranged from ~50–150 bp. A single SNP per locus was randomly selected to reduce linkage disequilibrium across sites and ensure sampling of independent SNP histories. The final dataset was composed of 18,672 (*A. ortonii*), 15,421 (*A. punctatus*), or 4,589 (*P. marmoratus*) unlinked SNPs. Genetic datasets used in all analyses were deposited in Dryad (available at dx.doi.org/10.5061/dryad.2v1p6).

Phylogeographic Structure and Demographic Syndromes. We first inferred phylogenetic relationships with singular value decomposition scores for species quartets (SVD quartets) (42), sampling all possible quartets and allowing for up to 30% of missing data. Node support was estimated with 1,000 bootstrap replicates. We then used sNMF 1.2 (37) to test the best-fit number of genetic clusters within each species (*k*) and to assign individuals to populations. We tested multiple *k* values (1–10), with 20 replicate runs for each *k* value and allowed a maximum of 30% missing data (each site was present in at least 70% of individuals). Robustness of the results was assessed by testing four values of the alpha regularization parameter (10, 100, 1,000, and 10,000).

Once we ensured that individuals from each spatial group (eastern Amazonia, western Amazonia, and northern Atlantic Forest) for each species did not violate the assumption of panmixia (based on the sNMF test of genetic clustering), we tested which historical demographic syndrome—instantaneous population expansion, instantaneous contraction, or constant size—best describes lizards in each region. For downstream site frequency spectrum (SFS)-based analyses, we used dadi 1.7 (43) to convert individual SNP data to an unpolarized SFS that summarizes patterns of site polymorphism across all sampled individuals within a population. The SNP data of each spatial group were down-projected to an SFS with equivalent sampling sizes across groups, allowing downstream aSFS analyses of groups composed of different numbers of sampled individuals (see below) while decreasing the effect of different levels of missing data between groups. Depending on the analysis, spatial groups of *A. punctatus* were down-projected to 10, 5, or 4 diploid individuals, *A. ortonii* groups were down-projected to five and four diploid individuals, and the *P. marmoratus* northern Atlantic Forest group was down-projected to four diploid individuals (see below and Dataset S4 for the number of SNPs and down-projection scheme used in each analysis). The number of individuals in each down-projecting scheme was chosen to maximize the number of sampled individuals while minimizing levels of missing data in each group.

To estimate best-fit demographic syndromes, we used *fastsimcoal2* 2.5 (38) to simulate 100,000 coalescent simulations per demographic syndrome (for a total of 300,000 simulations) for each sampling level per spatial group. We then used an ABC procedure to compare each observed SFS with the

appropriate simulations. Prior distributions used were time of instantaneous change ~*uniform* (*U*)(5 k, 1 million) generations ago, size change magnitude ~*U*(0.04, 0.2), with subsequent conversion to inverse in the case of contraction, current effective population size change for expansion ~*U*(100 k, 1 million), current effective population size change for constant size ~*U*(50 k, 500 k), and current effective population size change for contraction ~*U*(5 k, 100 k). An ABC model selection procedure was accomplished using the *R* package *abc* (44), using the model selection function *postpr()* to estimate the best-fit syndrome and the parameter estimation function *abc()* to infer posterior distributions for time, magnitude of population size change, and effective population size. Under ABC simple rejection sampling, we accepted the 1,500 (0.5%) simulations with the shortest Euclidian distance between the simulated and the empirical SFS. The model with the greatest posterior distribution then was selected as the best-fit demographic syndrome for each spatial group. To determine qualitatively whether tested models were discriminable based on the SFS, we visually inspected principal component analysis (PCA) plots based on a random selection of 100 simulated SFS under each model (for a total of 300 simulations). Moreover, to confirm that the best-fit model could generate the observed data, we conducted a PCA on the posterior-accepted simulated SFS, projected the empirical SFS into the principal components (PCs), and plotted the empirical data point, along with the accepted simulated data, on axes PC2 vs. PC1.

Estimating Magnitude of Synchronicity in Population Size Change. We tested the degree of synchronicity in population size changes across spatial groups through three sets of analyses. In analysis 1, we tested the degree of synchronicity in population size changes at a species level, comparing the three spatial groups within the better-sampled species *A. punctatus* and *A. ortonii* separately. Given the substantially greater sampling of *A. punctatus*, we down-projected the data of this species to 10 diploid individuals. In the case of *A. ortonii*, the data were down-projected to five diploid individuals. In analysis 2, we combined data from *A. punctatus* and *A. ortonii* spatial groups, all projected to five diploid individuals, to estimate the degree of synchronicity in population size shifts across all three geographic regions in both species. In analysis 3, we inferred the degree of synchronicity in demographic responses across the three species within the northern Atlantic Forest, a region for which enough sampled SNPs per individual of *P. marmoratus* were available. For this analysis, all three species in the northern Atlantic Forest were down-projected to four diploid individuals. In each analysis, we combined the empirical (observed) SFS of the spatial groups under consideration into an aSFS (22).

We then used an hABC procedure, which compares the observed aSFS with aSFS simulated under a hierarchical demographic model with varying degrees of synchronicity, to estimate (*i*) the proportion of groups in synchrony, ζ; (*ii*) the variance/mean of demographic change timing across spatial groups (with lower values signaling greater synchronicity), DI; and (*iii*) the timing of synchronous population size change (22). We performed 1 million coalescent simulations of the aSFS using *fastsimcoal2*, implementing the same prior distributions as the demographic syndrome analysis; the exception was the prior for ε in the expander populations, set to ~*U*(0.02, 0.2), and for current effective population size, set to ~*U*(500 k, 2 million) for expanders and ~*U*(50 k, 250 k) for contractors, because single-population analyses often had L-shaped posterior distributions for these parameters. The hyper-prior for ζ was distributed according to a discrete uniform prior across all possible values from a single spatial group (i.e., completely idiosyncratic) to all spatial groups (i.e., complete synchrony) within a synchronous pulse. We also implemented a time buffer to ensure that asynchronous or idiosyncratic spatial groups responded at >20,000 generations apart from the synchronous time. This strategy aimed to increase the identifiability of ζ by reducing the temporal proximity of asynchronous responses to spatial groups in synchrony. In analyses in which the spatial group-level analyses supported expansion in some spatial groups but contraction in others (Dataset S4), we built the aSFS in three steps. First, an aSFS was built based only on the SFS of the spatial groups found to have expanded. Then another aSFS was built based only on the SFS of groups found to have contracted. Lastly, these two aSFS were concatenated to form a single summary statistic vector. Simulated aSFS were constructed accordingly to each respective empirical aSFS. With this method we were able to reduce statistical noise resulting from improper model specification and conflicting population signals.

Following hABC hyper-parameter inference, we accepted the 1,500 simulations whose aSFS had the shortest Euclidian distance from the empirical aSFS, using the *R* package *abc*. The function *postpr()* was used to infer ζ, with each discrete value treated as a separate model, and the function *abc()* was used to estimate the remaining parameter summaries (i.e., DI and synchronous time). Posterior distributions then were estimated based on the values

of the retained simulations. As in the procedure for the spatial group-specific demographic syndrome analysis, we performed a PCA on the accepted simulations and plotted the simulated data with the empirical aSFS along the first two PCs to assess if the proposed scenarios could have generated the empirical aSFS. Furthermore, to assess hABC performance using the aSFS, we performed 50 leave-one-out cross-validations for the set of simulations per each empirical aSFS, with each cross-validation involving the extraction of a single simulation to act as a pseudo-observed dataset (POD) and using the remaining simulations for hABC estimation. This procedure was conducted using the functions *cv4postpr()* for ζ and *cv4abc()* for the parameter summaries, both contained in the R package *abc*. For each set of cross-validations, we calculated Pearson's correlation and the rms error between the known and estimated values across the 50 leave-one-out PODs. PCA plots based on the simulated SFS confirmed that the scenarios tested by the demographic analyses were generally discriminable (Figs. S1–S4). The PCA plots of the aSFS vectors calculated from the hABC rejection-sampled posterior, as well as from the aSFS calculated from the observed data, confirmed that best-fit models could generate the observed data. The leave-one-out cross-validation experiment indicated few biases and adequate accuracy in parameter estimates and model testing based on hABC analyses and the aSFS (Dataset S5).

Species Distribution Models to Inform Analyses of the Future Distribution of Genetic Diversity. To parameterize predictive models of future shifts in the spatial distribution of genomic diversity, we estimated migration rates and maximum carrying capacity at occupied sites from spatial demographic simulations that used friction and carrying capacity layers derived from SDMs projected into former climates. We used the empirical SNP data to validate the simulated demographic scenarios (and hence to enable the estimation of demographic parameters) by following multiple forward-in-time spatial demographic simulations with a corresponding backward-in-time genetic simulation. The simulations closest to the empirical genetic data were retained for estimation of posterior distributions of model parameters. Given the complexity of the analysis, we restricted this inference to the Atlantic Forest and to the two best-sampled species, *A. punctatus* and *A. ortonii*.

Species distribution models were generated in MaxEnt 3.3.3k (45), as implemented in SDMtoolbox 1.1c (46). We used museum records, data from collaborators, and data from our own fieldwork to compile occurrence records of *A. punctatus* and *A. ortonii*, which then were vetted for spatial and taxonomic accuracy. We then randomly selected one of multiple occurrence records per species within a 10-km radius using SDMtoolbox (46). The final dataset for SDM building was composed of 129 records of *A. punctatus* and 72 records of *A. ortonii* (Dataset S7). All models used eight standard bioclimatic variables summarizing patterns of precipitation and temperature, at a 2.5 arc-minute resolution (Bio1, 4, 10–12, 15–17 available at www.worldclim.org) (47). Models were built with occurrence points from the entire range of the species and later were clipped to the Atlantic Forest (−2.126 N, −59.567 W to −36.076 N, −34.717 W). Pseudoabsence (background) points were sampled from a minimum convex polygon defined as a 100-km buffer drawn around the occurrence localities (48).

To parameterize the SDMs properly, we evaluated the performance of various combinations of five feature classes (linear; linear and quadratic; hinge; linear, quadratic and hinge; and linear, quadratic, hinge, product and threshold), and 10 regularization multipliers (from 0.5 to 5, in increments of 0.5) (49). To this end, we evaluated the performance of SDMs built under each combination of model parameters through a geographically structured *k*-fold cross-validation (i.e., the occurrence records were partitioned into *k* equal geographically clustered subsamples, here *k* = 5, and the models were trained with four of the groups and then evaluated with the excluded group until all group combinations were run). Model fit was assessed through inspections of the omission rate, area under the curve (AUC), and model feature class complexity (46). After optimum model parameters were determined (those leading to the lowest omission rate, highest AUC, and lowest complexity, in the order listed), a final SDM was built with all occurrence sites. For both *A. punctatus* and *A. ortonii*, the best-fit models were parameterized with linear, quadratic, and hinge feature classes and a regularization multiplier of 0.5 and 1, respectively. The best resulting SDMs for *A. punctatus* and *A. ortonii* (of 250 SDMs with alternative parameter combinations for each species) show high predictive accuracy (average omission rates 0.320 and 0.243, respectively) and high average AUCs (0.758 and 0.918). These final models were used to infer the range of each anole into the past and future. When projecting to variable values outside the observed range, all projections of the response curves were reset ("clamped") to match the upper or lower values found in the study area (45).

Models of the paleodistribution of the species were derived with snapshot simulations of climate spanning the last 70 ky (at 1-ky time intervals back up to 22 kya, and before that at 2-ky time intervals, with 46 time periods in total) derived from the Hadley Centre Climate model (HadCM3) (50, 51). To project species ranges and genetic diversity under future climates, we used bioclimatic variables estimated from the Hadley Center model for the years 2030, 2050, 2070, and 2080 (HadGEN2-ES) (32), which is based on the RCP 6.0 emission scenario (31).

Estimating Carrying Capacity and Friction from SDMs. The SDMs generated under each former climatic period were rendered into two landscapes, friction and carrying capacity, for use in spatial demographic simulations (52, 53). The carrying capacity represents the maximum number of individuals that can occupy a grid cell at that time and is proportional to the suitability values given by the SDM. The friction values depict the relative difficulty of movement of individuals across different points in the landscape and are inversely proportional to the suitability inferred for the adjacent cells. To convert the SDMs into these friction and carrying capacity landscapes, we tested five transformation functions: linear, sigmoid (with two different inflection points), and binary (with two different cutoffs) (53). The sigmoid function best matched current distribution data. Conversion was performed with a normal cumulative distribution function, where the inflection point of the sigmoidal curve was 0.5 and the slope of the curve was 0.091 for *A. punctatus* and 0.073 for *A. ortonii*. These values were defined based on suitability values (from the SDM) measured at sites with known occurrences, where half of the SD equaled the slope of the curve (53).

Spatial Demographic Simulations for the Past. A total of 200,000 forward-in-time simulations of dispersal were performed under different migration rates and maximum carrying capacities. These 2D stepping-stone demographic colonizations (54) were simulated based on the per-deme maximum carrying capacity and migration limitations imposed by the friction and carrying capacity landscapes, using the program SPLATCHE 2 (55). In the demographic modeling, the colonization of the landscape proceeded in a generation-by-generation manner, from a predetermined ancestral source area(s) (see below). In each generation, population growth in each deme (i.e., an occupied cell) followed a logistic model characterized by a per-generation intrinsic growth rate (set to 0.2) and the time-specific SDM-informed maximum carrying capacity. This step was followed immediately by migration of individuals into neighboring demes, conditioned by the time-specific SDM-based friction of the landscape. The number of emigrants (dispersers) per generation from a given deme was modeled as a function of the migration rate (*m*, the proportion of individuals of a deme emigrating at each generation) and of the total number of occupants in that deme (which in turn depends on the local carrying capacity and on the population growth rate, under a logistic growth trend). A spatial resolution of *ca.* 30 km² (∼0.35°) was used for the demographic modeling because the spatial autocorrelation of the observed genetic data approached zero at this resolution [measured in SAM 4.0 using a spatial correlogram (56)].

To define the ancestral area from which spatial simulations would start, as well as the initial population density in those cells, we considered cells whose suitability score corresponded to the top 0.1 quartile of suitability values from the SDM projected to 70 kya [the oldest time period considered in our spatial demographic analyses (52)]. At the start of the simulations, each cell in which the species was considered to be present was assigned the maximum number of individuals (i.e., the maximum per deme carrying capacity). If the cell's actual carrying capacity, as informed by the corresponding projected SDM, was lower than the maximum capacity (i.e., if its suitability was lower than the maximum), the remaining individuals were distributed in neighbor cells. Because of computational limitations on the number of generations and on spatial resolution, a generation time of 10 y was used in the spatial demographic simulations. To adjust the results of the simulations to the more biologically plausible generation time of 1 y for anole lizards (57, 58), we multiplied the mutation, recombination, and growth rates by 10.

Spatial Genetic Simulations for the Past. To use the empirical data to validate the simulated demographic scenarios, and hence enable estimation of demographic parameters, each forward-in-time spatial demographic simulation was followed by a corresponding backward-in-time genetic simulation. The latter was parameterized by the spatially explicit demographic conditions simulated first. Specifically, the record of the per-generation movement of individuals and deme population sizes provided by the demographic simulations informed the probability of within-deme coalescent events and the probability of backward-in-time movement to neighboring demes of each sampled SNP. SNPs from focal populations were sampled from the resulting

genealogies (52, 53). The simulated genetic data matched the empirical genetic dataset used in this analysis: We simulated and sampled the same number of markers (4,000 SNPs) and the same number of individuals per sampled cell (15 sampling localities for *A. punctatus* and four for *A. ortonii*) (Dataset S8). Given the uncertainty in mutation rates for SNP data, we simulated SNPs into four equal groups (1,000 SNPs each) with mutation rates at each order between 1×10^{-5} to 1×10^{-8} mutations per site per generation. Rates of recombination were set to 0.822 cM/Mb based on genomic averages (59). Prior distributions were set as 3–5 for maximum landscape carrying capacity (*maxK*) and −3 to −0.5 for *m* (values in $\log_{10}$). Simulations were summarized into a total of 243 summary statistics for *A. punctatus* and 45 for *A. ortonii* with Arlequin v3.5 (60), including the statistics for between-site comparisons [e.g., mean number of alleles (*r*), *r* SD, mean heterozygosity (*H*), *H* SD, mean total *H*, mean number of pairwise differences, number of private polymorphic sites, and mean number of sites with segregating substitutions] and global descriptions (over all sites, e.g., total number of alleles, total number of polymorphic sites, total *H*). Because the use of a large number of summary statistics may reduce the accuracy of the ABC estimation as a result of high dimensionality (61), summary statistics were transformed into partial least squares (PLS) components (62) using the first 10,000 simulations as random calibration. After exploring the reduction of the rms errors associated with each additional PLS component for each parameter (63), we retained only the first nine PLS components. The 1,000 simulations (0.5%) closest to the empirical genetic data were retained for estimation of posterior distributions of model parameters (64), after adjustment with a general linear model (65). The fit of the model to the empirical data was evaluated by assessing the fraction of retained simulations that had likelihood smaller than or equal to that of the observed data (a small fraction suggests that the model does not fit well with the empirical data) (66). Accuracy of parameter estimation was assessed by calculating the coefficient of determination (R^2) between each parameter and the nine retained PLS components (67).

Estimating the Genetic Consequences of Future Climate Change. Once we estimated the demographic parameters for each species, we proceeded to map the distribution of genomic diversity currently and in the face of projected future climate change. To do so, we ran a final demographic simulation starting at 70 kya, which was ran forward until two points in time: the present (*ca.* 2010) and the year 2080. For each past time period, the posterior estimates (modes) of ancestral population size, migration rate, and carrying capacity derived from the historical analyses were used to parameterize the simulations. All other parameters, including growth rate, were kept at the values used for the initial spatial demographic simulations. Genetic constitution of every occupied locality was sampled at the end of each model run (on average, 1,560 and 183 grid cells for the present time and 1,508 and 172 cells for 2080, for *A. punctatus* and *A. ortonii*, respectively). Demographic and genetic simulations were repeated 100 times for each temporal scenario, through 20 replicate demographic models, each with five genetic simulation replicates (68). To measure predicted changes compared with present-day spatial patterns of genetic diversity, the genetic landscape predicted for 2080 was subtracted from that for the present day. Because output summary statistics of the simulated genetic data were highly correlated ($r = 0.81$, $P < 0.001$), we chose to present only mean allelic diversity here, which depicts the average allelic diversity (*r*) among the 4,000 simulated SNPs.

1. Avise JC, et al. (1987) Intraspecific phylogeography: The mitochondrial DNA bridge between population genetics and systematics. *Annu Rev Ecol Syst* 1987:489–522.
2. Avise JC (2000) *Phylogeography: The History and Formation of Species* (Harvard Univ Press, Cambridge, MA).
3. Moritz C, Patton JL, Schneider CJ, Smith TB (2000) Diversification of rainforest faunas: An integrated molecular approach. *Annu Rev Ecol Evol Syst* 31(1):533–563.
4. Schneider CJ, Cunningham M, Moritz C (1998) Comparative phylogeography and the history of endemic vertebrates in the Wet Tropics rainforests of Australia. *Mol Ecol* 7(4):487–498.
5. Pastorini J, Thalmann U, Martin RD (2003) A molecular approach to comparative phylogeography of extant Malagasy lemurs. *Proc Natl Acad Sci USA* 100(10):5879–5884.
6. Nicolas V, et al. (2008) Comparative phylogeography of two sibling species of forest-dwelling rodent (*Praomys rostratus* and *P. tullbergi*) in West Africa: Different reactions to past forest fragmentation. *Mol Ecol* 17(23):5118–5134.
7. Carnaval AC, Hickerson MJ, Haddad CFB, Rodrigues MT, Moritz C (2009) Stability predicts genetic diversity in the Brazilian Atlantic forest hotspot. *Science* 323(5915): 785–789.
8. Moritz C, et al. (2009) Identification and dynamics of a cryptic suture zone in tropical rainforest. *Proc Biol Sci* 276(1660):1235–1244.
9. Avila-Pires TCS, Mulcahy DG, Werneck FP, Sites JW (2012) Phylogeography of the teiid lizard *Kentropyx calcarata* and the sphaerodactylid *Gonatodes humeralis* (Reptilia: Squamata): Testing a geological scenario for the lower Amazon-Tocantins basins, Amazonia, Brazil. *Herpetologica* 68(2):272–287.
10. Dolman G, Joseph L (2012) A species assemblage approach to comparative phylogeography of birds in southern Australia. *Ecol Evol* 2(2):354–369.
11. Hewitt G (2000) The genetic legacy of the Quaternary ice ages. *Nature* 405(6789): 907–913.
12. Crawford AJ, Bermingham E, Carolina PS (2007) The role of tropical dry forest as a long-term barrier to dispersal: A comparative phylogeographical analysis of dry forest tolerant and intolerant frogs. *Mol Ecol* 16(22):4789–4807.
13. D'Horta FM, Cuervo AM, Ribas CC, Brumfield RT, Miyaki CY (2013) Phylogeny and comparative phylogeography of *Sclerurus* (Aves: Furnariidae) reveal constant and cryptic diversification in an old radiation of rain forest understorey specialists. *J Biogeogr* 40(1):37–49.
14. Demos TC, Kerbis Peterhans JC, Agwanda B, Hickerson MJ (2014) Uncovering cryptic diversity and refugial persistence among small mammal lineages across the Eastern Afromontane biodiversity hotspot. *Mol Phylogenet Evol* 71(1):41–54.
15. Lorenzen ED, Heller R, Siegismund HR (2012) Comparative phylogeography of African savannah ungulates. *Mol Ecol* 21(15):3656–3670.
16. Bagley JC, Johnson JB (2014) Testing for shared biogeographic history in the lower Central American freshwater fish assemblage using comparative phylogeography: Concerted, independent, or multiple evolutionary responses? *Ecol Evol* 4(9):1686–1705.
17. Smith BT, et al. (2014) The drivers of tropical speciation. *Nature* 515(7527):406–409.
18. Colwell RK, Rangel TF (2010) A stochastic, evolutionary model for range shifts and richness on tropical elevational gradients under Quaternary glacial cycles. *Philos Trans R Soc Lond B Biol Sci* 365(1558):3695–3707.
19. Papadopoulou A, Knowles LL (2016) Toward a paradigm shift in comparative phylogeography driven by trait-based hypotheses. *Proc Natl Acad Sci USA* 113:8018–8024.
20. Zamudio et al. (2016) Phenotypes in phylogeography: Species' traits, environmental variation, and vertebrate diversification. *Proc Natl Acad Sci USA* 113:8041–8048.
21. Hickerson MJ, Stahl E, Takebayashi N (2007) msBayes: Pipeline for testing comparative phylogeographic histories using hierarchical approximate Bayesian computation. *BMC Bioinformatics* 8(1):268.
22. Xue AT, Hickerson MJ (2015) The aggregate site frequency spectrum for comparative population genomic inference. *Mol Ecol* 24(24):6223–6240.
23. Pinto MA, et al. (2014) Genetic integrity of the dark European honey bee (*Apis mellifera mellifera*) from protected populations: A genome-wide assessment using SNPs and mtDNA sequence data. *J Apic Res* 53(2):269–278.
24. Streicher JW, et al. (2014) Diversification and asymmetrical gene flow across time and space: Lineage sorting and hybridization in polytypic barking frogs. *Mol Ecol* 23(13): 3273–3291.
25. Rittmeyer EN, Austin CC (2015) Combined next-generation sequencing and morphology reveal fine-scale speciation in Crocodile Skinks (Squamata: Scincidae: *Tribolonotus*). *Mol Ecol* 24(2):466–483.
26. Hijmans RJ, Graham CH (2006) The ability of climate envelope models to predict the effect of climate change on species distributions. *Glob Change Biol* 12(12):2272–2281.
27. Sinclair SJ, White MD, Newell GR (2010) How useful are species distribution models for managing biodiversity under future climates. *Ecol Soc* 15(8):1–13.
28. Brown JL, et al. (2016) Predicting the genetic consequences of future climate change: The power of coupling spatial demography, the coalescent, and historical landscape changes. *Am J Bot* 103(1):153–163.
29. Cheng H, et al. (2013) Climate change patterns in Amazonia and biodiversity. *Nat Commun* 4:1411.
30. Ledru M, Montade V, Cedex M, Cedex M, Pratique E (2015) Long-term spatial changes in the distribution of the Brazilian Atlantic Forest. *Biotropica* 48:159–169.
31. Van der Linden P, Mitchell JE (2009) *ENSEMBLES: Climate Change and its Impacts: Summary of Research and Results from the ENSEMBLES Project* (Met Office Hadley Centre, Exeter, UK).
32. IPCC (2015) *Intergovernmental Panel on Climate Change. Climate Change 2014: Mitigation of Climate Change* (Cambridge Univ Press, New York), Vol 3.

33. Waltari E, Schroeder R, McDonald K, Anderson RP, Carnaval A (2014) Bioclimatic variables derived from remote sensing: Assessment and application for species distribution modelling. *Methods Ecol Evol* 5(10):1033–1042.

34. Batalha-Filho H, Fjeldsa J, Fabre PH, Miyaki CY (2013) Connections between the Atlantic and the Amazonian Forest avifaunas represent distinct historical events. *J Ornithol* 154(1):41–50.

35. Costa LP (2003) The historical bridge between the Amazon and the Atlantic Forest of Brazil: A study of molecular phylogeography with small mammals. *J Biogeogr* 30(1):71–86.

36. Prates I, Rodrigues MT, Melo-Sampaio PR, Carnaval AC (2015) Phylogenetic relationships of Amazonian anole lizards (*Dactyloa*): Taxonomic implications, new insights about phenotypic evolution and the timing of diversification. *Mol Phylogenet Evol* 82(Pt A):258–268.

37. Frichot E, Mathieu F, Trouillon T, Bouchard G, François O (2014) Fast and efficient estimation of individual ancestry coefficients. *Genetics* 196(4):973–983.

38. Excoffier L, Dupanloup I, Huerta-Sánchez E, Sousa VC, Foll M (2013) Robust demographic inference from genomic and SNP data. *PLoS Genet* 9(10):e1003905.

39. Baker PA, et al. (2014) The emerging field of Geogenomics: Constraining geological problems with genetic data. *Earth Sci Rev* 135:38–47.

40. Elshire RJ, et al. (2011) A robust, simple genotyping-by-sequencing (GBS) approach for high diversity species. *PLoS One* 6(5):e19379.

41. Eaton DAR (2014) PyRAD: Assembly of de novo RADseq loci for phylogenetic analyses. *Bioinformatics* 30(13):1844–1849.

42. Chifman J, Kubatko L (2014) Quartet inference from SNP data under the coalescent model. *Bioinformatics* 30(23):3317–3324.

43. Gutenkunst RN, Hernandez RD, Williamson SH, Bustamante CD (2009) Inferring the joint demographic history of multiple populations from multidimensional SNP frequency data. *PLoS Genet* 5(10):e1000695.

44. Csilléry K, François O, Blum MGB (2012) Abc: An R package for approximate Bayesian computation. *Methods Ecol Evol* 3(3):475–479.

45. Phillips SJ, Anderson RP, Schapire RE (2006) Maximum entropy modeling of species geographic distributions. *Ecol Modell* 190(3-4):231–259.

46. Brown JL (2014) SDMtoolbox: A python-based GIS toolkit for landscape genetic, biogeography, and species distribution model analyses. *Methods Ecol Evol* 5(7):694–700.

47. Hijmans RJ, Cameron SE, Parra JL, Jones G, Jarvis A (2005) Very high resolution interpolated climate surfaces for global land areas. *Int J Climatol* 1978(15):1965–1978.

48. Barbet-Massin M, Jiguet F, Albert CH, Thuiller W (2012) Selecting pseudo-absences for species distribution models: How, where and how many? *Methods Ecol Evol* 3(2):327–338.

49. Shcheglovitova M, Anderson RP (2013) Estimating optimal complexity for ecological niche models: A jackknife approach for species with small sample sizes. *Ecol Modell* 269:9–17.

50. Carnaval AC, et al. (2014) Prediction of phylogeographic endemism in an environmentally complex biome. *Proc R Soc B* 281(1792):20141461.

51. Fuchs J, et al. (2013) Extending ecological niche models to the past 120,000 years corroborates the lack of strong phylogeographic structure in the crested drongo (*Dicrurus forficatus forficatus*) on Madagascar. *Biol J Linn Soc Lond* 108(3):658–676.

52. Knowles LL, Alvarado-Serrano DF (2010) Exploring the population genetic consequences of the colonization process with spatio-temporally explicit models: Insights from coupled ecological, demographic and genetic models in montane grasshoppers. *Mol Ecol* 19(17):3727–3745.

53. Brown JL, Knowles LL (2012) Spatially explicit models of dynamic histories: Examination of the genetic consequences of Pleistocene glaciation and recent climate change on the American Pika. *Mol Ecol* 21(15):3757–3775.

54. Kimura M, Weiss GH (1964) The stepping stone model of population structure and the decrease of genetic correlation with distance. *Genetics* 49(4):561–576.

55. Ray N, Currat M, Foll M, Excoffier L (2010) SPLATCHE2: A spatially explicit simulation framework for complex demography, genetic admixture and recombination. *Bioinformatics* 26(23):2993–2994.

56. Rangel TF, Diniz-Filho JAF, Bini LM (2010) SAM: A comprehensive application for spatial analysis in macroecology. *Ecography* 33(1):46–50.

57. Tollis M, Ausubel G, Ghimire D, Boissinot S (2012) Multi-locus phylogeographic and population genetic analysis of *Anolis carolinensis*: Historical demography of a genomic model species. *PLoS One* 7(6):e38474.

58. Muñoz MM, et al. (2013) Divergence in coloration and ecological speciation in the *Anolis marmoratus* species complex. *Mol Ecol* 22(10):2668–2682.

59. Dumont BL, Payseur BA (2008) Evolution of the genomic rate of recombination in mammals. *Evolution* 62(2):276–294.

60. Excoffier L, Lischer HE (2010) Arlequin suite ver 3.5: A new series of programs to perform population genetics analyses under Linux and Windows. *Mol Ecol Resour* 10(3):564–567.

61. Blum MG (2012) Approximate Bayesian computation: A nonparametric perspective. *J Am Stat Assoc* 105(491):1178–1187.

62. Boulesteix AL, Strimmer K (2007) Partial least squares: A versatile tool for the analysis of high-dimensional genomic data. *Brief Bioinform* 8(1):32–44.

63. Wegmann D, Leuenberger C, Excoffier L (2009) Efficient approximate Bayesian computation coupled with Markov chain Monte Carlo without likelihood. *Genetics* 182(4):1207–1218.

64. Beaumont MA, Zhang W, Balding DJ (2002) Approximate Bayesian computation in population genetics. *Genetics* 162(4):2025–2035.

65. Leuenberger C, Wegmann D (2010) Bayesian computation and model selection without likelihoods. *Genetics* 184(1):243–252.

66. Wegmann D, Leuenberger C, Neuenschwander S, Excoffier L (2010) ABCtoolbox: A versatile toolkit for approximate Bayesian computations. *BMC Bioinformatics* 11(1):116.

67. Neuenschwander S, Hospital F, Guillaume F, Goudet J (2008) quantiNemo: An individual-based program to simulate quantitative traits with explicit genetic architecture in a dynamic metapopulation. *Bioinformatics* 24(13):1552–1553.

68. Gehara M, Summers K, Brown JL (2013) Population expansion, isolation and selection: Novel insights on the evolution of color diversity in the strawberry poison frog. *Evol Ecol* 27(4):797–824.